Geophysical Research Letters

RESEARCH LETTER
10.1029/2024GL113789

Mixing Accounts for More Than Half of Biogeochemical Changes Along Mode Water Ventilation Pathways

M. Jutras[1], S. M. Bushinsky[1], I. Cerovečki[2], and N. Briggs[3]

[1]Department of Oceanography, SOEST, University of Hawai'i at Mnoa, Honolulu, HI, USA, [2]Scripps Institution of Oceanography, University of California San Diego, San Diego, CA, USA, [3]National Oceanography Centre, Southampton, UK

Key Points:

- More than half of observed changes in oxygen concentrations along mode waters ventilation pathways is due to mixing with surrounding waters
- The use of Apparent Oxygen Utilization overestimates respiration and biological carbon export in mode waters by a factor of up to two
- Observed oxygen to nitrate stoichiometric ratios that are not corrected for mixing should be termed *apparent stoichiometric ratios*

Supporting Information:

Supporting Information may be found in the online version of this article.

Correspondence to:

M. Jutras,
mjutras@hawaii.edu

Citation:

Jutras, M., Bushinsky, S. M., Cerovečki, I., & Briggs, N. (2025). Mixing accounts for more than half of biogeochemical changes along mode water ventilation pathways. *Geophysical Research Letters*, *52*, e2024GL113789. https://doi.org/10.1029/2024GL113789

Received 28 NOV 2024
Accepted 11 MAR 2025

Author Contributions:

Conceptualization: M. Jutras, S. M. Bushinsky, I. Cerovečki
Data curation: N. Briggs
Formal analysis: M. Jutras
Funding acquisition: S. M. Bushinsky
Methodology: M. Jutras, S. M. Bushinsky
Project administration: S. M. Bushinsky
Supervision: S. M. Bushinsky, I. Cerovečki
Visualization: M. Jutras
Writing – original draft: M. Jutras
Writing – review & editing: S. M. Bushinsky, I. Cerovečki, N. Briggs

Abstract Mode waters are critical for ocean ventilation and carbon sequestration. Using observations, we trace their subduction pathways and biogeochemical evolution. Solving modified mixing equations that account for respiration reveals that less than 50% of the oxygen changes along mode water ventilation pathways are due to respiration within the water mass, the rest being due to mixing with oxygen-poorer surrounding waters. Consequently, measured changes in oxygen or Apparent Oxygen Utilization overestimate respiration by a factor of up to two, as do derived biogeochemical quantities such as remineralized carbon. Measured nitrate changes either overestimate or underestimate remineralization depending on surrounding concentrations. Mean true respiration rates in mode waters range from −0.1 to −0.4 μmol $kg^{-1}yr^{-1}$. Applying a fixed stoichiometric ratio to this respiration, we find that the total carbon export is highest in Southern Ocean mode waters, while carbon remineralization rates are highest in subtropical mode waters.

Plain Language Summary In the ocean, surface waters connect with depth through subduction events, during which surface waters become denser and sink. When surface waters subduct, they transport carbon and oxygen into the ocean interior. Quantifying this transport is essential to constrain how much anthropogenic carbon is absorbed by the ocean, as well as how oxygen, essential to marine life, is supplied to the ocean interior. These quantities are, however, challenging to estimate from observations because the ocean is highly dynamic, with currents following complex 3-Dimensional paths and waters constantly mixing. In this study, we use observations from the growing network of autonomous profiling floats equipped with biogeochemical sensors and water samples collected from ships to track different water masses as they subduct. We then investigate whether changes in oxygen and nutrient concentrations are driven by biological or physical processes. We demonstrate that neglecting the effect of mixing, as is often done, can lead to overestimating respiration and biological carbon export by up to a factor of two.

1. Introduction

Mode waters play a crucial role in transporting carbon, oxygen, and nutrients from the ocean's surface to its interior. In doing so, they sequester anthropogenic carbon (Müller et al., 2023; Rhein et al., 2017), ventilate the oceans (Rhein et al., 2017), and fuel up to 75% of biological productivity in mid-latitudes (Hauck et al., 2018; Primeau et al., 2013; Sarmiento et al., 2004). It is thus crucial to understand how mode waters' properties evolve as these are advected into the ocean's interior and which processes govern changes in their biogeochemical properties. Mode waters form when intense winter heat loss at the surface causes convection, deepening the mixed layer and resulting in the subduction of surface waters (Styles et al., 2024; Suga et al., 2008). The deepening of the mixed layer generates low potential vorticity (PV) waters, which constitutes a good tracer for mode waters (Herraiz-Borreguero & Rintoul, 2011; McCartney, 1982). Once subducted, the waters follow 3D interior pathways that circulate around ocean basins, following local overturning and gyre circulation (Berglund et al., 2022; Li et al., 2021; Morrison et al., 2022, and references therein). The properties of mode waters change along their ventilation pathways due to physical and biogeochemical processes, including (a) re-ventilation events; (b) respiration (remineralization), which leads to a progressive depletion in oxygen and enrichment in dissolved inorganic carbon (DIC) and nutrients; and (c) diapycnal and isopycnal mixing (Billheimer et al., 2021; Broecker & Östlund, 1979; Herraiz-Borreguero & Rintoul, 2011; Koch-Larrouy et al., 2010). Tracking this evolution and identifying its different drivers has yet to be done from observations without resorting to ocean models.

Distinguishing between physical and biological drivers of biogeochemical property changes is crucial to obtain a mechanistic understanding of processes, but also to assess the limitations of traditional metrics such as Apparent Oxygen Utilization (AOU), the difference between saturation and measured oxygen concentration ($AOU = [O_2^{sat}]–[O_2^{obs}]$). AOU is biased due to undersaturation at the time of subduction (e.g., Bushinsky & Cerovečki, 2023; Bushinsky & Emerson, 2018; Fröb et al., 2016; Wolf et al., 2018), but also due to the effect of mixing with surrounding water masses (Ito et al., 2004). The combination of these biases causes AOU to overestimate true respiration by 25%–35% in models (Carter et al., 2020; Duteil et al., 2013) and causes Oxygen Utilization Rates (OUR), obtained by dividing AOU by age, to overestimate true respiration rates in subsurface waters and underestimate them in surface waters (e.g., Billheimer et al., 2021; Guo et al., 2023; Ono et al., 2001) because AOU and age are affected differently by advection and mixing (Koeve & Kähler, 2016). AOU is also used to derive quantities estimating ocean biogeochemical cycles, such as regenerated nutrients (Duteil et al., 2012; Ito & Follows, 2005), organic carbon export, net community production (Feely et al., 2004; Jenkins, 1982; Oschlies & Kähler, 2004), or even anthropogenic carbon uptake (Asselot et al., 2024; Williams et al., 2015), resulting in biases in these quantities (Billheimer et al., 2021; Feely et al., 2004; Ono et al., 2001).

In this study, we quantify the role of both physical and biological processes in modulating the evolution of biogeochemical properties along mode water ventilation pathways, for the first time based on observations alone. Unlike a more traditional framework where changes are interpreted along meridional or zonal transects (e.g., Fröb et al., 2016; Hahn et al., 2017; Müller et al., 2023; Schmidtko et al., 2017), we follow changes on 3D isopycnal pathways, along which water masses are advected following subduction.

2. Methods

2.1. Ventilation Pathways

To identify mode waters and ventilation pathways, we use a 1° × 1° gridded in situ temperature and salinity product derived from Core-Argo data (RG-Argo, Roemmich and Gilson, 2009) provided on 58 standard pressure levels (0–2,000 m) covering latitudes from 64.5°S to 79.5°N and the period from 2004 to 2023. From these, we derive potential vorticity, approximate geostrophic streamfunctions, and geostrophic velocities (McDougall & Klocker, 2010) on 0.1 kg m^{-3} neutral density surfaces (Jackett & McDougall, 1997). For each mode water, we define a mask (Figures 1a and 4a). First, we identify the region based on the literature (Table S1 in Supporting Information S1, Feucher et al., 2019; Hanawa & Talley, 2001). Second, we locate the mode water layers by finding the PV minimum in the water column (Figure S1 in Supporting Information S1). Thirdly, we create a mask where PV is below a threshold (Table S1 in Supporting Information S1) and volume exceeds 0.8×10^{12} m^3 per grid cell. The PV thresholds are determined during step 2 and through visual inspection of maps (Figure 1a). Only the North Atlantic Subpolar Mode Waters (NASPMW), which propagate outside the region covered by our data product (Brambilla & Talley, 2008), are not considered in this study. Since mode waters predominantly advect along geostrophic streamlines after subduction (Jones et al., 2016, Figure S2 in Supporting Information S1), we determine the ventilation pathways by following the streamlines that emanate from low PV regions (see Figure 1a for an example for the Pacific sector Subantarctic Mode Waters, $SAMW_{Pacific}$). The beginning of the pathway is determined as the location from which oxygen decreases steadily, indicating that the water is no longer in contact with the surface ocean.

To investigate biogeochemical changes along the identified pathways, we use two data sets: biogeochemical Argo (BGC-Argo) floats (Argo, 2024; Wong et al., 2020) and the Global Ocean Data Analysis Project Version 2 (GLODAPv2) v2022 ship-based data set (Lauvset et al., 2016; Olsen et al., 2016), which cover the last five decades. We select the observations that fall within the mask and neutral density bounds associated with each water mass (Figure 1a) and assign them a distance along the pathway based on the closest streamline.

2.2. Disentangling the Sources of Biogeochemical Changes Along Mode Water Pathways

Next, we distinguish physical and biological processes causing the evolution in biogeochemical properties along the pathways. We first compute the mean water properties and standard deviation (σ) in distance bins of 1,000 km, within each 0.1 kg m^{-3} neutral density layer. We do this for oxygen and nitrate concentrations (Figures 2a and 2b), but also temperature and salinity, from which we compute oxygen saturation for AOU.

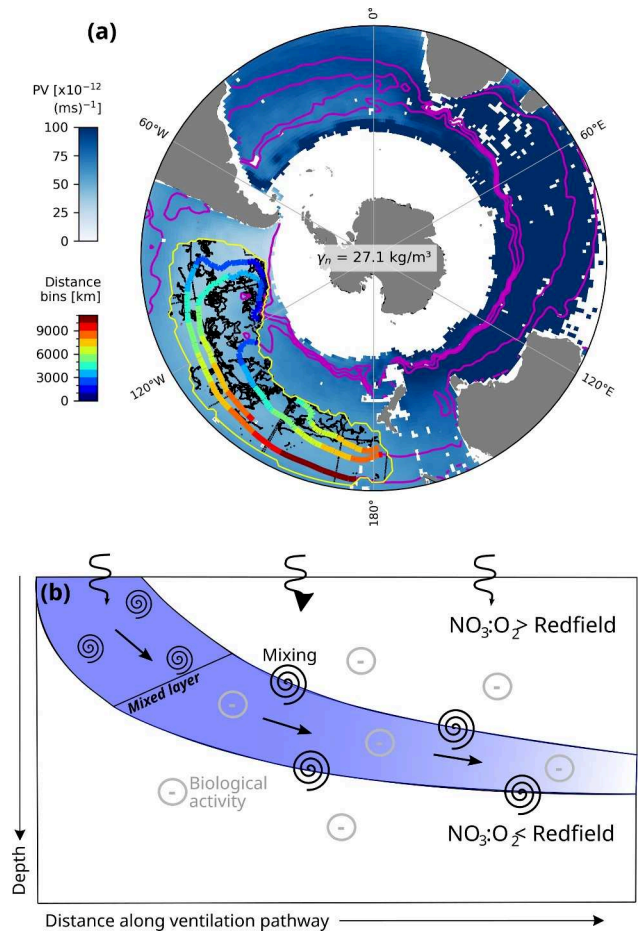

Figure 1. (a) Potential vorticity (PV) in the Southern Ocean for the 27.1–27.2 kg m^{-3} neutral density layer, from the RG-Argo product. Pink lines contour streamlines. The yellow contour delineates the mask used to define the Pacific SAMW water mass on this layer, and the black dots represent individual measurements falling within this mask. Streamlines within the water mass are colored according to the distance along the pathway. (b) Schematic of processes affecting biogeochemical properties along ventilation pathways.

We then solve, for each bin i, mixing equations modified to include the effect of respiration/remineralization (Figure 3f, Jutras et al., 2020; Tomczak, 1981). The last equation ensures mass conservation,

$$f_{i-1}C_{i-1} + f_{above}C_{above} + f_{below}C_{below} = C_i \quad (1a)$$

$$f_{i-1}O_{2,i-1} + f_{above}O_{2,above} + f_{below}O_{2,below} + R = O_{2,i} \quad (1b)$$

$$f_{i-1}N_{i-1} + f_{above}N_{above} + f_{below}N_{below} + r_{N:O2}R = N_i \quad (1c)$$

$$f_{i-1} + f_{above} + f_{below} = 1 \quad (1d)$$

where C is a conservative property (here, temperature or salinity), O_2 is the dissolved oxygen concentration, N is the nitrate concentration, labels *above* and *below* designate surrounding layers ±0.1 kg m^{-3}, R is the respiration in units µmol kg^{-1} of oxygen and $r_{N:O2} = 16{:}{-}154$ is the stoichiometric ratio of nitrate to oxygen during respiration (Hedges et al., 2002). We provide values for $C_{i/i-1/above/below}$, $O_{2,i/i-1/above/below}$ and $N_{i/i-1/above/below}$ (Figures 3d and 3e), and obtain two outputs: (a) the fraction of each water mass contributing to the sampled water parcel (f_{i-1}, f_{above}, f_{below}) and (b) the respiration that occurred within the distance bin (R). Note that R represents what we could call the respiration *within the water mass*, in contrast to *integrated* respiration, which would include the respiration that occurs in surrounding water masses before they mix in. For the system to be exactly determined (four

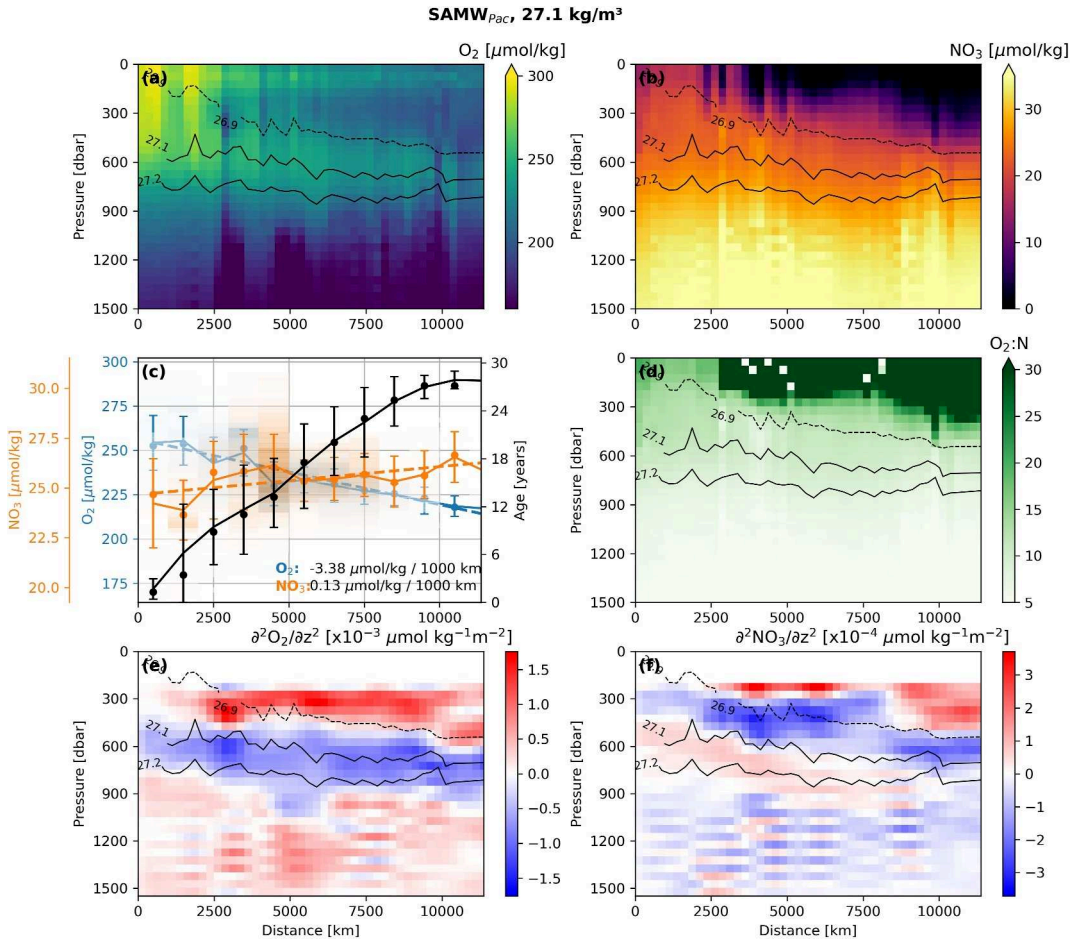

Figure 2. SAMW$_{Pacific}$ biogeochemical evolution. (a and b) Section plots of gridded, averaged, and interpolated Argo and GLODAP data along the pathway (colored lines in Figure 1a) of (a) dissolved oxygen concentration and (b) nitrate concentration. Three isopycnal layers compose the SAMW$_{Pacific}$. The dashed line delineates the top of the water mass (γ_n = 26.9 kg/m^3), while the black solid lines delineate an example layer used to produce panel (c) and Figure 3 (γ_n = 27.1–27.2 kg/m^3). (c) Mean dissolved oxygen concentrations, nitrate concentrations, and age along the pathway on that isopycnal. Orange and blue shadings indicate the density distribution of the Argo data. Dotted lines show linear regressions, with the slopes indicated at the bottom right. (d) Section plot of the dissolved oxygen to nitrate ratio along the pathway. (e and f) Second vertical derivative of (e) dissolved oxygen and (f) nitrate concentrations. Notice the very different scales for the two fields. For (e) and (f), we use 250 km distance bins and 50 m depth bins and smooth the field using a 3 × 3 bin window. See Figure S6–S12 in Supporting Information S1 for similar figures for other mode waters.

unknowns and four variables), we solve it separately for temperature and salinity and average the two solutions, which are similar (Figure S3 in Supporting Information S1). We solve the system using a Monte Carlo approach. We run 10,000 iterations, applying random perturbations distributed within the standard deviation σ associated with each variable (see Text S1 in Supporting Information S1). From the outputs of Equation 1, we retrieve the change in dissolved oxygen or nitrate attributable to either mixing or respiration:

$$\Delta\Lambda^{respiration} = R \tag{2a}$$

$$\Delta\Lambda^{mixing} = f_{above}\Lambda_{above} + f_{below}\Lambda_{below} - \left(f_{above} + f_{below}\right)\Lambda_i \tag{2b}$$

where Λ stands for oxygen or nitrate concentrations. Finally, we can estimate the amount of carbon being remineralized along the whole pathway by summing over distance bins i: $C_{remin} = \sum_i R_i V_i$ where V_i is the volume from the RG-Argo product.

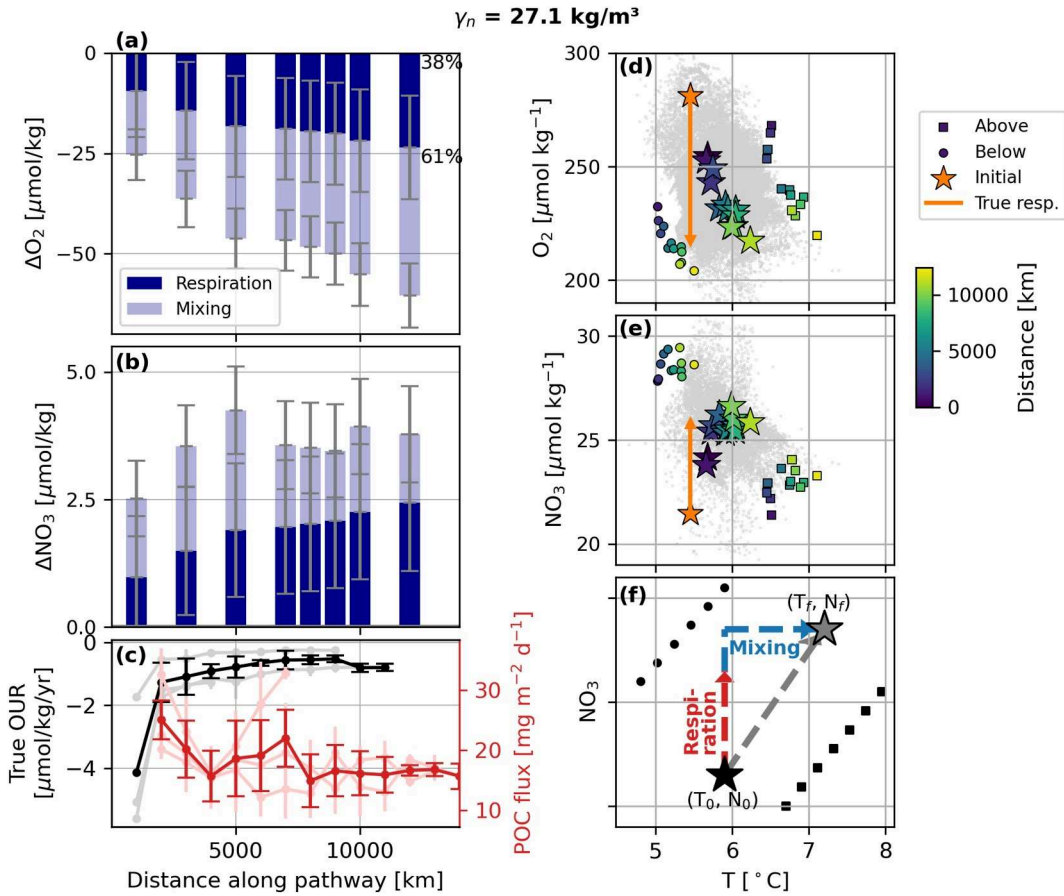

Figure 3. Causes of biogeochemical changes in the $SAMW_{Pacific}$ 27.1–27.2 kg/m^3 layer. Cumulative (a) oxygen and (b) nitrate change due to respiration (full color) and to mixing with surrounding water masses (light color) along the pathway. Distance bins with no clear increase in oxygen are combined with the next bin. (c) Mean true respiration rate (black) and Particulate Organic Matter (POC) flux estimated from Argo backscatter data (see Tables S1 and S2 in Supporting Information S1) in the three $SAMW_{Pacific}$ density layers, along the ventilation pathway. Light colors show the individual layers. (d–f) Mixing diagrams for dissolved (d) oxygen and (e) nitrate. Orange stars indicate the properties at the beginning of the ventilation pathway. Orange lines indicate the change expected from respiration only. The other stars indicate the mean water properties along distance bins, colored by distance. The squares and circles show the same for the waters above and below, respectively ($\gamma_n \pm 0.1$ kg m^{-3}). The gray points in the background illustrate individual measurements. (f) Schematic mixing diagram. From an initial set of properties (black star), respiration increases nitrate (red dashed line), and mixing (blue dashed lines) with surrounding water masses (black lines) tilts this displacement left or right.

2.3. Estimating Ventilation Time

We estimate the ventilation time along the identified ventilation pathways using Lagrangian tracking experiments performed with the OceanParcels tool for Python (Van Sebille et al., 2023). Virtual particles are released at the beginning of the pathways, on the target isopycnals and every 100 m in the horizontal (Figure 2b and Figure S4 in Supporting Information S1) and are advected on isopycnals with a fourth-order Runge-Kutta scheme using the velocities calculated from the RG-Argo product. Using the same mapping method as for water properties (Section 2.1), we find a strong relationship between age and distance, which we use to estimate age along streamlines.

3. Results

3.1. Evolution Along Ventilation Pathways

Throughout Section 3, we illustrate our approach using, as an example, the γ_n = 27.1–27.2 kg m^{-3} neutral density layer of the $SAMW_{Pacific}$ and then compare to various layers and mode waters globally (Figure 4a). At the beginning of the $SAMW_{Pacific}$ ventilation pathway, oxygen levels are 35–50 μmol kg^{-1} below saturation.

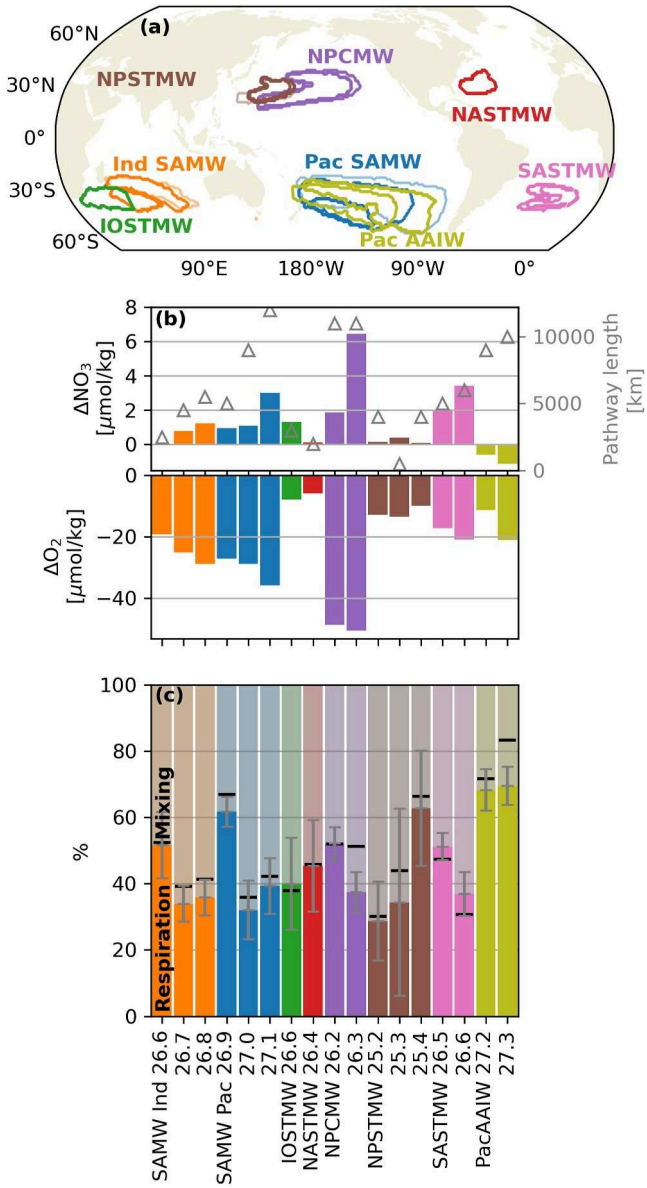

Figure 4. Net biogeochemical changes in different mode waters. (a) Masks used to delineate the different mode waters (defined on 0.1 kg m^{-3} neutral density bounds, Section 2.1). The water mass labels stand for the following: SAMW Pac: Pacific sector Subantarctic Mode Waters; SAMW Ind: Indian Ocean sector Subantarctic Mode Waters; IOSTMW: Indian Ocean Subtropical Mode Waters; NASTMW: North Atlantic Subtropical Mode Waters; NPCMW: North Pacific Central Mode Waters; NPSTMW: North Pacific Substropical Mode Waters; SASTMW: South Atlantic Subtropical Mode Waters; PacAAIW: Pacific sector Antarctic Intermediate Waters. (b) Net observed nitrate (top) and oxygen (bottom) change between the beginning and the end of the ventilation pathways. Gray triangles provide the length of the pathways. (c) Percentage of the net oxygen change due to local respiration (dark color) and mixing (light color, see Section 2.2). The black bar indicates the percentage relative to AOU instead of net oxygen change.

Globally, across mode waters, deviations from saturation at the beginning of the pathway range from 20 μmol kg^{-1} below saturation in the deepest Indian Ocean SAMW ($SAMW_{Indian}$) to 57 μmol kg^{-1} below saturation in the deepest North Pacific Central Mode Waters (NPCMW). This departure from saturation results from a combination of undersaturation at the time of ventilation, biological respiration, and mixing occurring during and after subduction.

Following ventilation in the Pacific sector of the Southern Ocean, $SAMW_{Pacific}$ are modified as they take on average 18 years to propagate northwestward into the interior Pacific Ocean (Figures 1a and 2a–2c). At the end of their ~10,000 km pathway, they have lost about 30 μmol kg^{-1} of oxygen, slightly less AOU, and gained about 2 μmol kg^{-1} of nitrate (Figures 3 and 4c, Table S2 in Supporting Information S1). Dissolved oxygen concentrations in that water mass decline at a rate of −2.7 to −6.7 μmol kg^{-1} per 1,000 km, depending on the layer (Figures 2c and 4b). Nitrate increases at a rate of 0.1–0.3 μmol kg^{-1} per 1,000 km. Temperature and salinity also increase, suggesting mixing with surrounding water masses (Figures 3d and 3e).

Across mode waters, the mean rate of oxygen loss and nitrate gain along the pathway varies, ranging for oxygen from −1.7 μmol kg^{-1} per 1,000 km in the North Pacific Subtropical Mode Waters (NPSTMW) to −10.1 μmol kg^{-1} per 1,000 km in the $SAMW_{Indian}$, and for nitrate from +0.1 μmol kg^{-1} per 1,000 km in the $SAMW_{Pacific}$ to +1.7 μmol kg^{-1} per 1,000 km in the Indian Ocean Subtropical Mode Waters (IOSTMW, Figure 4b). The stoichiometric ratio in the change of oxygen relative to nitrate varies across water masses and differs from the expected Redfield stoichiometric ratios (Figure S5 in Supporting Information S1). The ratios are generally lower than the standard values, except in the IOSTMW, NASPMW and SASTMW where they are higher.

3.2. Causes of Biogeochemical Changes

Solving Equation 1 shows that local respiration accounts for 30%–50% of the net measured oxygen or AOU change along the $SAMW_{Pacific}$ ventilation pathway, depending on the density layer (Figures 3a and 4c), while mixing explains the balance. This proportion varies by up to 40% along the pathway, ranging from 90% near the beginning to 50% by the end of the pathway in the lightest layer (Figure 3a and Figure S14 in Supporting Information S1). Mixing lowers oxygen concentrations, just like respiration does (Figure 3a), but the effect on nitrate is variable, increasing it in some regions and decreasing it in others (Figure 3b).

Across water masses, the proportion of biogeochemical changes attributed to mixing and respiration remains relatively constant, with respiration accounting for 29%–62% of the observed net oxygen change along mode waters ventilation pathways (Figure 4c). Respiration also explains only 30%–83% of the net change in AOU along the pathways, again highlighting how AOU differs from true respiration.

Dividing the obtained true respiration (Equation 1a) by age estimates from the tracer release experiments, we calculate new estimates of true oxygen utilization rates (OUR_{True}). For $SAMW_{Pacific}$, we find OUR_{True} values ranging from 0.3 to 0.1 μmol $kg^{-1}yr^{-1}$ from the lighter to denser layers (Figure S13 and Table S2 in Supporting Information S1). These numbers can be challenging to compare with published estimates, which do not follow individual water masses. However, OUR_{True} estimates match those made within the same region that correct for

mixing (Koeve & Kähler, 2016, model-based) and are lower than estimates that do not apply this correction (0.12–4.9 μmol $kg^{-1}yr^{-1}$, Feely et al. (2004); 25 μmol $kg^{-1}yr^{-1}$, Martz et al. (2008)). Across mode waters, OUR_{True} values range from 0.5 to 6.0 μmol $kg^{-1}yr^{-1}$ (Table S2 in Supporting Information S1), again generally lower than published estimates (see Figure S14 in Supporting Information S1).

Our calculated mixing rates, when expressed as $F_{Mix} = \kappa \frac{\partial [O_2]}{\partial z}$, imply diffusion coefficients κ on the order of $10^{-4}m^2s^{-1}$ in the upper layers, and $10^{-5}m^2s^{-1}$ in the deeper layers. These values are consistent with current estimates for the ocean (Whalen et al., 2012), providing support to our approach.

4. Discussion

4.1. Control on the Relative Roles of Mixing and Respiration

We demonstrated that the relative importance of mixing versus respiration varies for different variables and water masses (Figures 3a, 3b, and 4c), but what causes these variations? The differential impact of mixing on oxygen and nitrate (Section 3.1, Figures 3a and 3b) is related to the properties of surrounding waters: since mode waters bring reoxygenated waters into the ocean's interior, they are surrounded by waters with lower oxygen concentrations (Figure 2a). Turbulent diapycnal mixing is to a first order proportional to the vertical gradients in concentrations (Equation 1), so mixing with these surrounding waters will lower oxygen concentrations (Figure 2e). In contrast, because mode waters are formed in regions where surface waters are richer in nitrate compared to lower latitudes (where surface waters are nitrate depleted), nitrate concentrations increase with depth in this portion of the water column (Figure 2b) and hence offer a different response to mixing than oxygen. Mixing with waters above will decrease nitrate concentrations, while mixing with waters below will increase them, making the effect of mixing on nitrate more sensitive to the balance of mixing with above and below (Figure 2f).

While the relative proportion of respiration to mixing in biogeochemical evolution appears to be primarily controlled by water properties, true respiration rates appear to follow organic matter availability, decreasing along the ventilation pathways (Figure 3c and Figure S14 in Supporting Information S1). This decrease is consistent with the progressive remineralization of subducted organic matter and with a decrease in the amount of sinking organic matter along the pathways (Figure 3c and Figure S14 in Supporting Information S1) observed from Argo backscatter data (Text S3 in Supporting Information S1).

4.2. Derived Biogeochemical Properties

Not accounting for mixing leads to biases in biogeochemical quantities derived from changes in biogeochemical variables or from AOU. For instance, stoichiometric ratios during respiration/remineralization are sometimes calculated from measured changes in oxygen and nitrate (e.g., Anderson & Sarmiento, 1994). We suggest that these measured ratios should be termed *apparent stoichiometric ratios*, since mixing modifies the measured stoichiometric ratios in ways that do not follow respiration alone. Mixing with surface waters, which are nitrate-depleted and oxygen-enriched (Figures 2a, 2b, 3d, and 3e), will increase the measured ratios, while mixing with deeper waters, where the ambient oxygen-to-nitrate ratio is generally low (Figure 2d), will decrease the measured ratios (Figure S5 in Supporting Information S1). This is consistent with studies showing that mixing with cold waters causes deviations from the Redfield ratio in the Southern Ocean (Ishizu & Richards, 2013) and that mixing homogenizes nutrient concentration and phenotype distribution, thus smoothing stoichiometric ratios (Deutsch & Weber, 2012; Weber & Deutsch, 2010). We also suggest that mixing could help explain observed anomalies in the amount of nutrients remineralized relative to carbon remineralization and oxygen consumption in subtropical waters (e.g., Fawcett et al., 2018; Letscher & Villareal, 2018).

The impact of mixing also propagates into metrics used to analyze the marine carbon cycle. For instance, AOU is directly used to partition regenerated and pre-formed nitrate concentrations (Duteil et al., 2012; Ito & Follows, 2005). These estimates are then used to evaluate the efficiency of the soft-tissue pump (Ito & Follows, 2005), but are also integrated over depth and stoichiometrically converted to carbon to estimate biological carbon fluxes, storage, and production (Feely et al., 2004; Jenkins, 1982; Oschlies & Kähler, 2004). It has been suggested that not accounting for mixing will thus overestimate biological carbon storage (Feely et al., 2004; Ono et al., 2001). We quantify this overestimation to be 45%–75% in mode waters (Section 3.2). Remineralized carbon estimates are further utilized to predict expected carbon concentrations, which are then compared with measured values to estimate anthropogenic carbon concentrations (e.g., Asselot et al., 2024; Williams et al., 2015).

Neglecting the effects of mixing could therefore lead to an underestimation of the anthropogenic carbon content in mode waters.

Hence, our method offers a way to avoid these biases. By applying a C_{org}:O_2 stoichiometric ratio to our estimates of true respiration, we obtain the first observation-based estimates of remineralized carbon, providing a measure of biological carbon storage by specific water masses (excluding advected carbon). Considering a ratio of −106:154 (Hedges et al., 2002), we find that $SAMW_{Pacific}$ acquires 0.16 Pg of remineralized carbon between subduction and the end of its pathway, at a rate of 0.2–2.4 mgC $m^{-3}yr^{-1}$. Published estimates within the same region are generally larger (0.1–3.4 mgC $m^{-3}yr^{-1}$, Feely et al. (2004); 13–45 mgC $m^{-3}yr^{-1}$, Martz et al. (2008)), as expected, since they do not account for the effect of mixing. Our results moreover provide important insights into the role of different water masses in carbon storage in the ocean. Comparing all mode waters suggests that subtropical mode waters play a particularly important role in biological carbon storage, accumulating respired carbon at rates of 1.5–9.5 mgC $m^{-3}yr^{-1}$ (Table S2 in Supporting Information S1) compared to less than 2.5 mgC $m^{-3}yr^{-1}$ in subpolar mode waters. However, over the entire pathways, $SAMW_{Pacific}$ accumulates the highest amount of biological carbon (0.16 PgC), while subtropical mode waters, which have shorter pathways, accumulates less (0.002–0.006 PgC). These comparisons highlight the benefit of a water mass approach and explicit determination of mixing rates to constrain ocean biogeochemical cycles.

4.3. Limitations and Uncertainties

This study relies on a number of assumptions. We assume that water is advected by the geostrophic flow, neglecting the eddy-induced flow. Jones et al. (2016) showed that using geostrophic streamlines was a good assumption for tracking SAMW pathways. We also assume that the ocean interior is sufficiently adiabatic to follow water masses after subduction by tracking along density lines. In the RG-Argo product, the path of the potential vorticity minimum (i.e., the core of mode waters) and approximate geostrophic streamlines align well once away from the subduction zone (Figure S2 in Supporting Information S1), supporting our assumptions. In addition, we average data from all years and employ fixed masks to define water masses, thereby providing a mean climatological picture and neglecting potential temporal variability or trends in the water properties and pathways. In the Southern Ocean between 2004 and 2008, PV only shows small variations that would marginally affect the periphery of our masks (Figures 4a and 5 in Zhang et al., 2021). We also confirm that the data distribution does not induce biases due to uneven spatial sampling by comparing the evolution of physical properties from the more extensive core-Argo data set and from the BGC-Argo data set, which are similar. In this study, we did not explicitly include isopycnal mixing. We argue that isopycnal mixing within the water masses is implicitly taken into account, acting perpendicularly to the streamlines along which we perform the analysis. We however neglect isopycnal mixing at the edges of our masks. The small surface area of the edges compared to the whole water masses should make this contribution negligible, but we acknowledge that it could represent a significant source (Billheimer et al., 2021) or sink of oxygen in some water masses and its contribution should be explored in the future. Lastly, we assume fixed stoichiometric ratios during remineralization, although these ratios vary with location and depth (e.g., Martiny et al., 2013; Sauterey & Ward, 2022).

5. Conclusion

Ventilation pathways are often conceptualized as conduits, transporting water from the surface to the ocean interior with minimal interactions with the surroundings. Our results add important nuance to this framework. By applying a mixing analysis to observational data, we demonstrate that, in mode waters, mixing with oxygen-deficient waters reduces oxygen levels during transport to the ocean interior, biasing AOU. The impact of mixing on nitrate evolution varies depending on properties of surrounding waters. We provide true respiration estimates that correct for both undersaturation at the time of subduction and for mixing, revealing that true respiration accounts for less than half of the observed changes in oxygen along mode water subduction pathways (Figures 1b and 4c), or, in other words, that AOU or net changes in oxygen overestimate respiration by about 50% in mode waters. We use these estimates of true respiration to obtain estimates of true remineralized carbon, which can be half those based directly on measured biogeochemical changes (e.g., on AOU or difference to pre-formed nutrients). We identify SAMW as accumulating the highest amounts of respired carbon from ventilation to complete mixing with other water masses, while subtropical mode waters exhibit the highest biological carbon

accumulation rates per unit time. Correcting for mixing is thus essential for properly constraining oceanic biogeochemical cycles, and requires a characterization of the water masses surrounding a water mass of interest.

Our analysis also demonstrates that BGC-Argo and GLODAP data can be used to characterize the evolution of biogeochemical properties along the three-dimensional ventilation pathways of specific water masses. This opens the door to observation-based estimations of transport of biogeochemical properties by specific water masses, which have for now mostly been evaluated from models (Hauck et al., 2018).

Finally, while we focused on mode waters for their critical role in linking the surface to interior ocean, the discrepancy between true biological activity and observed biogeochemical is likely different for other types of water masses, in magnitude and in sign. The approach presented here could be applied to any water mass to derive such estimates.

Data Availability Statement

The BGC-Argo data can be accessed through the GDAC (https://biogeochemical-argo.org/data-access.php), and the GLODAP data can be downloaded directly from their website (https://glodap.info/index.php/merged-and-adjusted-data-product-v2-2023/). The scripts used to extract the data and apply the water mass analysis are available on Zenodo (Jutras, 2025). This repository also contains four processed data sets: (a) gridded global potential vorticity and approximate geostrophic streamlines on neutral density levels, (b) ventilation pathways associated with each water mass, (c) mean ventilation time along the pathways, based on Lagrangian tracking experiments, and (d) biogeochemical evolution along pathways and results of the water mass analysis, including the data required to reproduce Figures 1, 3, and 4.

Acknowledgments
This work was funded through a Natural Sciences and Engineering Research Council (NSERC) of Canada postdoctoral fellowship attributed to MJ, through NASA Grant 80NSSC22K0156 (SMB, IC, MJ), NSF OCE Grant 2049631 (SMB, IC), NASA Grant 80NSSC19K1115 (IC), and through UK National Environment Research Council (NERC) Grant NE/X008657/1 (NB). The authors would like to thank the two reviewers for their insightful and thorough recommendations. MJ would like to thank D. König for providing python functions to calculate mixed layer depth. This is SOEST contribution 11918.

References

Anderson, L., & Sarmiento, J. L. (1994). Redfield ratios of remineralization determined by nutrient data analysis. *Global Biogeochemical Cycles*, *8*(1), 65–80. https://doi.org/10.1029/93gb03318

Argo. (2024). Argo float data and metadata from global data assembly centre (Argo GDAC). https://doi.org/10.17882/42182

Asselot, R., Carracedo, L. I., Thierry, V., Mercier, H., Bajon, R., & Pérez, F. F. (2024). Anthropogenic carbon pathways towards the North Atlantic interior revealed by Argo-O_2, neural networks and back-calculations. *Nature Communications*, *15*(1), 1630. https://doi.org/10.1038/s41467-024-46074-5

Berglund, S., Döös, K., Groeskamp, S., & McDougall, T. J. (2022). The downward spiralling nature of the North Atlantic subtropical gyre. *Nature Communications*, *13*(1), 2000. https://doi.org/10.1038/s41467-022-29607-8

Billheimer, S., Talley, L. D., & Martz, T. R. (2021). Oxygen seasonality, utilization rate, and impacts of vertical mixing in the eighteen degree water region of the Sargasso Sea as observed by profiling biogeochemical floats. *Global Biogeochemical Cycles*, *35*(3). https://doi.org/10.1029/2020gb006824

Brambilla, E., & Talley, L. D. (2008). Subpolar mode water in the northeastern Atlantic: 1. Averaged properties and mean circulation. *Journal of Geophysical Research*, *113*(C4), 2006JC004062. https://doi.org/10.1029/2006jc004062

Broecker, W. S., & Östlund, H. G. (1979). Property distributions along the $\sigma_0 = 26.8$ isopycnal in the Atlantic Ocean. *Journal of Geophysical Research*, *84*(C3), 1145–1154. https://doi.org/10.1029/jc084ic03p01145

Bushinsky, S. M., & Cerovečki, I. (2023). Subantarctic mode water biogeochemical formation properties and interannual variability. *AGU Advances*, *4*(2), e2022AV000722. https://doi.org/10.1029/2022av000722

Bushinsky, S. M., & Emerson, S. R. (2018). Biological and physical controls on the oxygen cycle in the Kuroshio Extension from an array of profiling floats. *Deep Sea Research Part I: Oceanographic Research Papers*, *141*, 51–70. https://doi.org/10.1016/j.dsr.2018.09.005

Carter, B. R., Feely, R. A., Lauvset, S. K., Olsen, A., DeVries, T., & Sonnerup, R. (2020). Preformed properties for marine organic matter and carbonate mineral cycling quantification. *Global Biogeochemical Cycles*, *35*(1), e2020GB006623. https://doi.org/10.1029/2020gb006623

Deutsch, C., & Weber, T. (2012). Nutrient ratios as a tracer and driver of ocean biogeochemistry. *Annual Review of Marine Science*, *4*(1), 113–141. https://doi.org/10.1146/annurev-marine-120709-142821

Duteil, O., Koeve, W., Oschlies, A., Aumont, O., Bianchi, D., Bopp, L., et al. (2012). Preformed and regenerated phosphate in ocean general circulation models: Can right total concentrations be wrong? *Biogeosciences*, *9*(5), 1797–1807. Publisher: Copernicus GmbH. https://doi.org/10.5194/bg-9-1797-2012

Duteil, O., Koeve, W., Oschlies, A., Bianchi, D., Galbraith, E., Kriest, I., & Matear, R. (2013). A novel estimate of ocean oxygen utilisation points to a reduced rate of respiration in the ocean interior. *Biogeosciences*, *10*(11), 7723–7738. Publisher: Copernicus GmbH. https://doi.org/10.5194/bg-10-7723-2013

Fawcett, S. E., Johnson, K. S., Riser, S. C., Van Oostende, N., & Sigman, D. M. (2018). Low-nutrient organic matter in the Sargasso Sea thermocline: A hypothesis for its role, identity, and carbon cycle implications. *Marine Chemistry*, *207*, 108–123. https://doi.org/10.1016/j.marchem.2018.10.008

Feely, R. A., Sabine, C. L., Schlitzer, R., Bullister, J. L., Mecking, S., & Greeley, D. (2004). Oxygen utilization and organic carbon remineralization in the upper water column of the Pacific Ocean. *Journal of Oceanography*, *60*(1), 45–52. https://doi.org/10.1023/b:joce.0000038317.01279.aa

Feucher, C., Maze, G., & Mercier, H. (2019). Subtropical mode water and Permanent pycnocline properties in the world ocean. *Journal of Geophysical Research: Oceans*, *124*(2), 1139–1154. https://doi.org/10.1029/2018jc014526

Fröb, F., Olsen, A., Våge, K., Moore, G. W., Yashayaev, I., Jeansson, E., & Rajasakaren, B. (2016). Irminger Sea deep convection injects oxygen and anthropogenic carbon to the ocean interior. *Nature Communications*, *7*(1), 13244. https://doi.org/10.1038/ncomms13244

Guo, H., Kriest, I., Oschlies, A., & Koeve, W. (2023). Can oxygen utilization rate be used to track the long-term changes of aerobic respiration in the mesopelagic Atlantic ocean? *Geophysical Research Letters*, *50*(13), e2022GL102645. https://doi.org/10.1029/2022gl102645

Hahn, J., Brandt, P., Schmidtko, S., & Krahmann, G. (2017). Decadal oxygen change in the eastern tropical North Atlantic. *Ocean Science*, *13*(4), 551–576. https://doi.org/10.5194/os-13-551-2017

Hanawa, K., & Talley, L. D. (2001). Mode waters. In G. Siedler, J. Church, & J. Gould (Eds.), *Ocean circulation and climate: Observing and modelling the Global Ocean*. Academic Press. number 77.

Hauck, J., Lenton, A., Langlais, C., & Matear, R. (2018). The fate of carbon and nutrients exported out of the Southern Ocean. *Global Biogeochemical Cycles*, *32*(10), 1556–1573. https://doi.org/10.1029/2018gb005977

Hedges, J. I., Baldock, J. A., Gélinas, Y., Lee, C., Peterson, M. L., & Wakeham, S. G. (2002). The biochemical and elemental compositions of marine plankton: A NMR perspective. *Marine Chemistry*, *78*(1), 47–63. https://doi.org/10.1016/s0304-4203(02)00009-9

Herraiz-Borreguero, L., & Rintoul, S. R. (2011). Subantarctic mode water: Distribution and circulation. *Ocean Dynamics*, *61*(1), 103–126. https://doi.org/10.1007/s10236-010-0352-9

Ishizu, M., & Richards, K. J. (2013). Relationship between oxygen, nitrate, and phosphate in the world ocean based on potential temperature: Biogeochemical Parameters. *Journal of Geophysical Research: Oceans*, *118*(7), 3586–3594. https://doi.org/10.1002/jgrc.20249

Ito, T., & Follows, M. J. (2005). Preformed phosphate, soft tissue pump and atmospheric CO_2. *Journal of Marine Research*, *63*(4), 813–839. https://doi.org/10.1357/0022240054663231

Ito, T., Follows, M. J., & Boyle, E. A. (2004). Is AOU a good measure of respiration in the oceans? *Geophysical Research Letters*, *31*(17), 1–4. https://doi.org/10.1029/2004gl020900

Jackett, D. R., & McDougall, T. J. (1997). A neutral density variable for the world's oceans. *Journal of Physical Oceanography*, *27*(2), 237–263. https://doi.org/10.1175/1520-0485(1997)027<0237:andvft>2.0.co;2

Jenkins, W. J. (1982). Oxygen utilization rates in North Atlantic subtropical gyre and primary production in oligotrophic systems. *Nature*, *300*(5889), 246–248. https://doi.org/10.1038/300246a0

Jones, D. C., Meijers, A. J., Shuckburgh, E., Sallée, J.-B., Haynes, P., McAufield, E. K., & Mazloff, M. (2016). How does subantarctic mode water ventilate the Southern Hemisphere subtropics? *Journal of Geophysical Research: Oceans*, *121*(9), 6558–6582. https://doi.org/10.1002/2016jc011680

Jutras, M. (2025). mathildejutras/ventilation-pathways-BGC: v1 [Software]. https://doi.org/10.5281/zenodo.14816522

Jutras, M., Dufour, C. O., Mucci, A., Cyr, F., & Gilbert, D. (2020). Temporal changes in the causes of the observed oxygen decline in the St. Lawrence Estuary. *Journal of Geophysical Research: Oceans*, *125*(12), 1–20. https://doi.org/10.1029/2020jc016577

Koch-Larrouy, A., Morrow, R., Penduff, T., & Juza, M. (2010). Origin and mechanism of subantarctic mode water formation and transformation in the Southern Indian Ocean. *Ocean Dynamics*, *60*(3), 563–583. https://doi.org/10.1007/s10236-010-0276-4

Koeve, W., & Kähler, P. (2016). Oxygen utilization rate (OUR) underestimates ocean respiration: A model study. *Global Biogeochemical Cycles*, *30*(8), 1166–1182. https://doi.org/10.1002/2015gb005354

Lauvset, S. K., Key, R. M., Olsen, A., van Heuven, S., Velo, A., Lin, X., et al. (2016). A new global interior ocean mapped climatology: The 1° × 1° GLODAP version 2. *Earth System Science Data*, *8*(2), 325–340. https://doi.org/10.5194/essd-8-325-2016

Letscher, R. T., & Villareal, T. A. (2018). Evaluation of the seasonal formation of subsurface negative preformed nitrate anomalies in the subtropical North Pacific and North Atlantic. *Biogeosciences*, *15*(21), 6461–6480. https://doi.org/10.5194/bg-15-6461-2018

Li, Z., England, M. H., Groeskamp, S., Cerovečki, I., & Luo, Y. (2021). The Origin and fate of subantarctic mode water in the Southern Ocean. *Journal of Physical Oceanography*. https://doi.org/10.1175/jpo-d-20-0174.1

Martiny, A. C., Pham, C. T. A., Primeau, F. W., Vrugt, J. A., Moore, J. K., Levin, S. A., & Lomas, M. W. (2013). Strong latitudinal patterns in the elemental ratios of marine plankton and organic matter. *Nature Geoscience*, *6*(4), 279–283. https://doi.org/10.1038/ngeo1757

Martz, T. R., Johnson, K. S., & Riser, S. C. (2008). Ocean metabolism observed with oxygen sensors on profiling floats in the South Pacific. *Limnology & Oceanography*, *53*(5part2), 2094–2111. https://doi.org/10.4319/lo.2008.53.5_part_2.2094

McCartney, M. S. (1982). The subtropical recirculation of Mode Waters. *Journal of Marine Research*, *40*, 427–464.

McDougall, T. J., & Klocker, A. (2010). An approximate geostrophic streamfunction for use in density surfaces. *Ocean Modelling*, *32*(3–4), 105–117. https://doi.org/10.1016/j.ocemod.2009.10.006

Morrison, A. K., Waugh, D. W., Hogg, A. M., Jones, D. C., & Abernathey, R. P. (2022). Ventilation of the Southern Ocean pycnocline. *Annual Review of Marine Science*, *14*(1), 405–430. https://doi.org/10.1146/annurev-marine-010419-011012

Müller, J. D., Gruber, N., Carter, B., Feely, R., Ishii, M., Lange, N., et al. (2023). Decadal trends in the oceanic storage of anthropogenic carbon from 1994 to 2014. *AGU Advances*, *4*(4), e2023AV000875. https://doi.org/10.1029/2023av000875

Olsen, A., Key, R. M., Van Heuven, S., Lauvset, S. K., Velo, A., Lin, X., et al. (2016). The global ocean data analysis project version 2 (GLODAPv2)—An internallyconsistent data product for the world ocean. *Earth System Science Data*, *8*(2), 297–323. https://doi.org/10.5194/essd-8-297-2016

Ono, T., Midorikawa, T., Watanabe, Y. W., Tadokoro, K., & Saino, T. (2001). Temporal increases of phosphate and apparent oxygen utilization in the subsurface waters of western subarctic Pacific from 1968 to 1998. *Geophysical Research Letters*, *28*(17), 3285–3288. https://doi.org/10.1029/2001GL012948

Oschlies, A., & Kähler, P. (2004). Biotic contribution to air-sea fluxes of CO_2 and O_2 and its relation to new production, export production, and net community production. *Global Biogeochemical Cycles*, *18*(1), 2003GB002094. https://doi.org/10.1029/2003gb002094

Primeau, F. W., Holzer, M., & DeVries, T. (2013). Southern Ocean nutrient trapping and the efficiency of the biological pump. *Journal of Geophysical Research: Oceans*, *118*(5), 2547–2564. https://doi.org/10.1002/jgrc.20181

Rhein, M., Steinfeldt, R., Kieke, D., Stendardo, I., & Yashayaev, I. (2017). Ventilation variability of Labrador Sea water and its impact on oxygen and anthropogenic carbon: A review. *Philosophical Transactions of the Royal Society A: Mathematical, Physical & Engineering Sciences*, *375*(2102), 20160321. https://doi.org/10.1098/rsta.2016.0321

Roemmich, D., & Gilson, J. (2009). The 2004–2008 mean and annual cycle of temperature, salinity, and steric height in the global ocean from the Argo Program. *Progress in Oceanography*, *82*(2), 81–100. https://doi.org/10.1016/j.pocean.2009.03.004

Sarmiento, J. L., Gruber, N., Brzezinski, M. A., & Dunne, J. P. (2004). High-latitude controls of thermocline nutrients and low latitude biological productivity. *Nature*, *427*(6969), 56–60. https://doi.org/10.1038/nature02127

Sauterey, B., & Ward, B. A. (2022). Environmental control of marine phytoplankton stoichiometry in the North Atlantic Ocean. *Proceedings of the National Academy of Sciences of the United States of America*, *119*(1), e2114602118. https://doi.org/10.1073/pnas.2114602118

Schmidtko, S., Stramma, L., & Visbeck, M. (2017). Decline in global oceanic oxygen content during the past five decades. *Nature*, *542*(7641), 335–340. https://doi.org/10.1038/nature21399

Styles, A. F., MacGilchrist, G. A., Bell, M. J., & Marshall, D. P. (2024). Spatial and temporal patterns of Southern Ocean ventilation. *Geophysical Research Letters*, *51*(4), e2023GL106716. https://doi.org/10.1029/2023gl106716

Suga, T., Aoki, Y., Saito, H., & Hanawa, K. (2008). Ventilation of the North Pacific subtropical pycnocline and mode water formation. *Progress in Oceanography*, *77*(4), 285–297. https://doi.org/10.1016/j.pocean.2006.12.005

Tomczak, M. (1981). A multi-parameter extension of temperature/salinity diagram techniques for the analysis of non-isopycnal mixing. *Progress in Oceanography*, *10*(3), 147–171. https://doi.org/10.1016/0079-6611(81)90010-0

Van Sebille, E., Kehl, C., Lange, M., Delandmeter, P., & The Parcels Contributors. (2023). Parcels (v2.4.2) [Sotfware]. https://doi.org/10.5281/zenodo.8010997

Weber, T. S., & Deutsch, C. (2010). Ocean nutrient ratios governed by plankton biogeography. *Nature*, *467*(7315), 550–554. https://doi.org/10.1038/nature09403

Whalen, C. B., Talley, L. D., & MacKinnon, J. A. (2012). Spatial and temporal variability of global ocean mixing inferred from Argo profiles. *Geophysical Research Letters*, *39*(18). https://doi.org/10.1029/2012GL053196

Williams, N. L., Feely, R. A., Sabine, C. L., Dickson, A. G., Swift, J. H., Talley, L. D., & Russell, J. L. (2015). Quantifying anthropogenic carbon inventory changes in the Pacific sector of the Southern Ocean. *Marine Chemistry*, *174*, 147–160. https://doi.org/10.1016/j.marchem.2015.06.015

Wolf, M. K., Hamme, R. C., Gilbert, D., Yashayaev, I., & Thierry, V. (2018). Oxygen saturation surrounding deep-water formation events in the Labrador Sea from Argo-O_2 data. *Global Biogeochemical Cycles*, *32*(4), 635–653. Publisher: Wiley Online Library. https://doi.org/10.1002/2017gb005829

Wong, A. P. S., Wijffels, S. E., Riser, S. C., Pouliquen, S., Hosoda, S., Roemmich, D., et al. (2020). Argo data 1999–2019: Two million temperature-salinity profiles and subsurface velocity observations from a global array of profiling floats. *Frontiers in Marine Science*, *7*. Frontiers. https://doi.org/10.3389/fmars.2020.00700

Zhang, Y., Du, Y., Qu, T., Hong, Y., Domingues, C. M., & Feng, M. (2021). Changes in the subantarctic mode water properties and Spiciness in the Southern Indian Ocean based on argo observations. *Journal of Physical Oceanography*, *51*, 2203–2221. https://doi.org/10.1175/jpo-d-20-0254.1